Self-assembled nanoparticle spirals from two-dimensional compositional banding in thin films

Dinesh K. Venkatachalam, Neville H. Fletcher, Dinesh K. Sood, and Robert G. Elliman[a)]
Department of Electronic Materials Engineering, Research School of Physics and Engineering, The Australian National University, Canberra, Australian Capital Territory 0200, Australia

(Received 11 March 2009; accepted 4 May 2009; published online 28 May 2009)

A self-assembly process is reported in which spiral patterns of gold nanoparticles form on silicon surfaces during the epitaxial crystallization of thin gold-silicon alloy layers. This behavior is observed only for gold concentrations above a critical value and is shown to result from two-dimensional compositional banding of a liquid alloy layer during the crystallization process. The compositional banding consists of alternate gold-rich and silicon-rich alloy bands, which are shown to be a direct consequence of free energy minimization, the band spacing being that which gives the maximum diffusive composition-separation rate. Gold nanoparticles subsequently form by Ostwald ripening on the surface of the gold-rich bands to give rise to the observed spiral patterns.
 [DOI: 10.1063/1.3143666]

The interaction of metals with amorphous-silicon (*a*-Si) is a subject of considerable fundamental and technological interest. For example, many metals are known to induce low temperature crystallization of *a*-Si (Ref. 1–5) and this is of use for converting deposited *a*-Si films into large-grained polycrystalline materials for photovoltaic applications.[6] Among the various metals, gold (Au) is of particular interest due to the fact that the gold-silicon system is a simple eutectic with no intermetallic phases and has a low eutectic temperature (363 °C at composition of 18 at. % Si). This was the first metallic alloy found to exhibit a glassy solid phase and remains one of the most puzzling amorphous solids. Despite the apparent simplicity of the bulk Au–Si binary phase diagram, the existence of a deep eutectic and low eutectic temperature can lead to interesting behavior, including unusual layering and surface crystallization observed in bulk liquid alloys at the eutectic composition.[7] Over the past few years, significant progress has been made in developing various templated[8] and nontemplated solution-based synthesis[9–12] and purification schemes for producing uniform populations of metallic nanoparticles. However, an important technological challenge that remains is to develop effective ways to self-assemble these nanoscale components on an arbitrary solid surface over large length scales. Here we report the evolution of self-assembled spirals of gold nanoparticles on silicon.

For all experiments, single crystal *p*-type (100)-oriented, silicon substrates were implanted with 20 keV gold ions to fluences in the range 2×10^{16}–4×10^{16} ions/cm^2 at room temperature using a metal vapor vacuum arc (MEVVA) ion source. This produced a near-surface *a*-Si/Au alloy layer of thickness ~25 nm. Following implantation, the samples were annealed in a rapid thermal annealing furnace at temperatures of 450–750 °C for 30 s or *in situ* in a scanning electron microscope (SEM). High purity argon was used as a carrier gas and the flow rate was maintained at 100 cm^3/min throughout the course of the short annealing cycles. SEM was also employed for *ex situ* observation of the self-organization on the silicon surface.

The evolution of the Au-implanted Si layer depends on the initial gold concentration.[13] Samples implanted to an initial peak Au concentration of less than 38 at. % and annealed at 580 °C for 10 min display random distributions of Au-rich nanoparticles on the silicon surface.[14] However, above this critical concentration, the system evolves into more complicated self-assembled structures such as those shown in Fig. 1. In this case, as we discuss below, the evolution involves three stages: compositional banding of the Au:Si layer to form alternate Au-rich and Si-rich bands around a central Au-rich particle, nucleation and growth of Au-rich dendritic phases or nanoparticles on the surface above the Au-rich bands, and two-dimensional Ostwald-ripening of the resulting nanoparticle spiral distributions.

The images in Fig. 1 correspond to the second stage of this process in which spiral bands of Au-rich phases form on the sample surface around a central particle. At lower temperatures, the spirals consist of dendritic phases, as shown in Fig. 1(a) and reported by others.[3] At higher temperatures, they consist of well-defined nanoparticles, as shown in Fig. 1(b). In both cases, the patterns are observed to form around a large Au-rich particle.

In order to understand the mechanism underlying the formation of the spiral patterns, their evolution was moni-

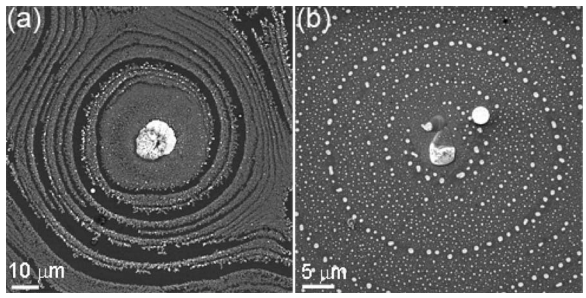

FIG. 1. Backscattered scanning electron micrographs of a (100) silicon sample ion-implanted with 20 keV Au ions to a fluence of 4×10^{16} Au/cm^2 after annealing for 30 s at temperatures (a) 540 °C and (b) 750 °C.

[a)]Author to whom correspondence should be addressed. Electronic mail: rob.elliman@anu.edu.au.

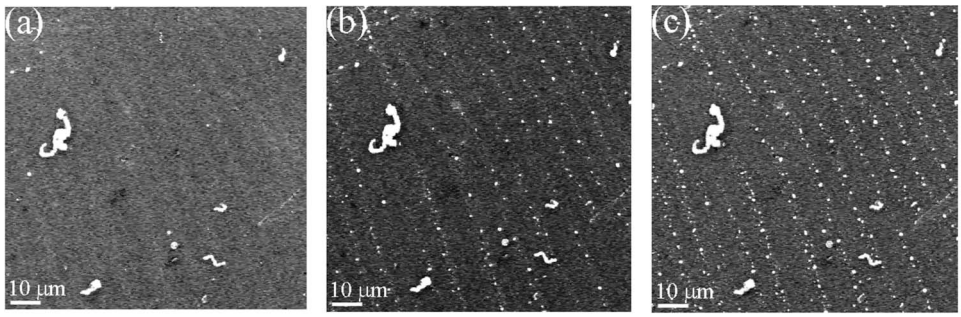

FIG. 2. Secondary electron micrographs showing time dependent nucleation of gold nanoparticles during isothermal annealing of 4×10^{16} Au/cm^2 in silicon (100) *in situ* in a SEM at 650 °C: (a) snapshot recorded at time $t=5$ s, (b) $t=60$ s, and (c) $t=180$ s. The bright bands are gold-rich and the dark bands are silicon-rich.

tored *in situ* in a SEM under isothermal annealing conditions. Figures 2(a)–2(c) show SEM images of a sample implanted with 4×10^{16} Au/cm^2 during annealing at 650 °C. The early stages of phase separation in the thin-film alloy layers are already evident after just 5 s, as shown in Fig. 2(a). The eutectic layer is expected to be molten at this temperature and the compositional bands are observed to form a spiral pattern around a central gold particle that is out of the field of view. Note that the spacing of the bands is of order 10 μm, suggesting a diffusion length for gold of this order. As the compositional banding occurs on a time scale of order 10 s, this implies a gold diffusivity of order 10^{-5} cm^2 s^{-1}, which is typical for the diffusion of impurities in liquid silicon.[15] This initial separation of the gold-silicon alloy layer into alternate gold- and silicon-rich bands appears to be analogous to the lamellaelike growth observed in bulk eutectic phases.[16,17] With increasing annealing time, gold-rich nanoparticles form on the sample surface above the gold-rich alloy bands, as shown in Fig. 2(b). The areal density of these particles then increases with increasing annealing time for times between 60 and 180 s [Fig. 2(c)].

The various evolutionary stages of the gold nanoparticle spirals are represented schematically in Figs. 3(a)–3(d). This is most easily discussed with reference to the phase diagram in Fig. 3(e), assuming a particular implant fluence (4×10^{16} Au/cm^2) and annealing temperature (650 °C). For this case, the initial gold implant produces a thin (25 nm) *a*-Si layer at the surface of a silicon wafer containing a Gaussian distribution of Au [Fig. 3(a)], with a peak gold concentration of 76 at. %. As the sample is heated to 650 °C, gold diffuses rapidly throughout the amorphous layer to form a uniform alloy layer with a gold concentration of ~50 at. %, as depicted in Fig. 3(b). This corresponds to point 1 on the phase diagram. During subsequent annealing, the amorphous layer crystallizes via solid-phase epitaxy and becomes thinner, as shown in Fig. 3(c). As it thins, the gold concentration in the layer increases and continues to increase to the point where the layer melts (i.e., an Au concentration of ~70 at. % for samples annealed at 650 °C, as represented by point 2 on the phase diagram). Once molten, the layer continues to crystallize via liquid-phase epitaxy, further concentrating the gold. This continues until the Au concentration exceeds a concentration of ~85 at. %, point 3 on the phase diagram, at which point the liquid layer becomes metastable with respect to the precipitation of gold particles. The nucleation and growth of a gold particle within the layer is expected to deplete the surrounding region of gold and initiate the compositional banding process [Fig. 3(d)].

There are three dominant thermodynamic quantities that are expected to drive the compositional banding process: the first is the difference E_1 in bulk free energy between the initial uniform eutectic phase and the two separated phases, the second is the difference E_2 in total surface free energy (that of the interface between the film and the substrate plus that of the interface of the film with the surrounding gas) between these structures, and the third is the free energy E_3 associated with the formation of the interface or composition gradient between the separated Au-rich and Si-rich phases. The total free energy is then $E_1+E_2-E_3$ where all these energies need to be considered per unit area. If a sinusoidal

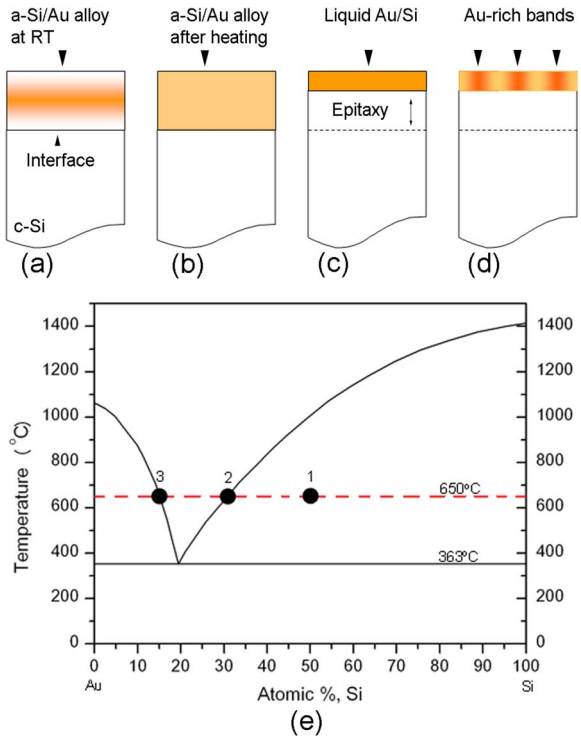

FIG. 3. (Color online) [(a)–(d)] Schematic representation of the various stages of the banded growth of thin *a*-Si/Au alloy. Specifically, (a) as-implanted sample showing the initial *a*-Si layer and implanted Au distribution, (b) layer during initial stages of annealing in which Au diffuses throughout the *a*-Si layer, (c) layer after solid phase epitaxy has reduced the layer to the point where the Au concentration is sufficient to cause melting, and (d) precipitation of a Au particle and subsequent compositional banding of the liquid Au:Si alloy layer. (e) The Au–Si phase diagram showing the evolution of a sample implanted with 20 keV Au to a fluence of 4×10^{16} Au cm^{-2} during annealing at 650 °C. The significance of points 1–3 is discussed in the text.

variation in composition is introduced, as illustrated in Fig. 3(d), thus separating the film into parallel bands, then the balance between these three free energy components determines the band separation that will develop most quickly. If the bands are too narrow and closely spaced, then there will be many interfaces per unit area so that the contribution of E_3 will be large and the total driving energy therefore small. If the band separation is very large, then the inhibiting contribution of E_3 will be small but the bands will develop slowly because of the large diffusion distances involved. There is therefore a particular band spacing, depending upon the parameters E_1, E_2, E_3 and the thickness of the film, for which bands will develop most rapidly, and this spacing will therefore dominate the pattern. Further details of this analysis will be given elsewhere[18] but a significant result is that the spacing of the bands can be expressed as

$$w = \frac{2E_3 h}{E_2 + E_1 h},$$

where w is the spacing of the bands and h is the thickness of the film. Since $E_3 > 0$, the detailed behavior will depend upon the signs of E_1 and E_2.

Compositional banding is expected to be initiated by a nucleation event that perturbs the local in-plane Au:Si distribution. The observation of a central Au-rich particle in the middle of each spiral pattern strongly suggests that the presence of such a particle acts to initiate the banding process. The bands will then tend to develop as rings around this nucleation point, forming at a particular point and growing in a progressive manner around the ring circumference. The circumferential growth of Au-rich bands is not expected to form perfect rings because the region in the vicinity of the bands is depleted of Au. Therefore, as the ends of an incomplete and growing Au-rich band approach each other, they are separated by a Au-depleted region, making exact junction unlikely. Instead the two ends grow past each other, separated by a distance comparable to the ring spacing and thereby leading to the observed spiral patterns. In addition, since nucleation is likely to occur in several different places, spiral patterns can interact, and depletion of the mixed phase will make them avoid each other, leading to complex "swirl" patterns, as often found. However, details of these processes are complicated and beyond the scope of the current discussion.

Once the spiral patterns of nanoparticles have formed, their subsequent evolution is determined by a two-dimensional Ostwald ripening processes. For the samples discussed in detail above, the areal density of the spirals increases, and the average diameter (distance from the large central particle to the outermost complete ring) decreases, with increasing annealing temperature. The density of spirals increases from 100 spirals/mm^2 at 525 °C to 400 spirals/mm^2 at 750 °C, with corresponding decrease in the diameter from 105 μm at 525 °C to 40 μm at 750 °C. Since the larger particle at the origin has a lower equilibrium solute concentration surrounding it than do the smaller particles in the rings, this initiates a radial diffusion process in which the ring particles tend to dissolve and the gold solute is transferred to the central particle. There is, however, a subtle refinement to this process for, if the particles in a given ring are disappearing, then the equilibrium solute concentration in the vicinity of that ring will increase and, as well as leading to diffusional transfer to the central particle, there will also be diffusional transfer to the neighboring larger ring, causing its particles to increase in size. This problem can readily be defined and solved numerically to provide insight into the ring evolution at long times and shows that some rings disappear, thus increasing the average ring spacing.[18]

In summary, we have shown that spiral patterns of gold nanoparticles can form on a silicon surface by a self-assembly process during annealing of Au-implanted silicon samples. A model for this behavior has been presented in which the spirals result from the spontaneous separation of a liquid Au–Si eutectic layer into alternating bands of gold-rich and silicon-rich composition. These bands form around an initial Au-rich precipitate that acts to perturb the local in-plane Au:Si distribution. During further annealing Au-rich nanoparticles nucleate and grow on the Si surface above the Au-rich bands to form spiral patterns of Au-rich nanoparticles. These patterns continue to evolve during annealing through the growth of some rings at the expense of others.

We thank P. Evans and D. Button for MEVVA implantation at Australian Nuclear Science Technology Organization under an AINSE Grant No. AINGRA05155P. We thank S.K. Bhargava at RMIT University for the financial support to D.K.V. to carry out initial stages of this research. We also thank T. Bostrom at Queensland University of Technology for providing access to the hot-stage SEM. We thank the ARC Australian Research Network for Advanced Materials and the Australian Research Council Nanotechnology Network for the student scholarship for collaborative research.

[1] L. Hultman, A. Robertsson, H. T. G. Hentzell, I. Engström, and P. A. Psaras, J. Appl. Phys. **62**, 3647 (1987).
[2] C. Hayzelden and J. L. Batstone, J. Appl. Phys. **73**, 8279 (1993).
[3] B. Bokhonov and M. Korchagin, J. Alloys Compd. **312**, 238 (2000).
[4] S. Y. Yoon, J. Y. Oh, C. O. Kim, and J. Jang, Solid State Commun. **106**, 325 (1998).
[5] R.-Y. Yang, M.-H. Weng, C.-T. Liang, Y.-K. Su, and S.-L. Shy, Jpn. J. Appl. Phys., Part 2 **45**, L1146 (2006).
[6] R. P. Nair and M. Zou, Surf. Coat. Technol. **203**, 675 (2008).
[7] O. G. Shpyrko, R. Streitel, V. S. K. Balagurusamy, A. Y. Grigoriev, M. Deutsch, B. M. Ocko, M. Meron, B. Lin, and P. S. Pershan, Science **313**, 77 (2006).
[8] F. Yan and W. A. Goedel, Nano Lett. **4**, 1193 (2004).
[9] C. Stowell and B. A. Korgel, Nano Lett. **1**, 595 (2001).
[10] L. Magagnin, V. Bertani, P. L. Cavallotti, R. Maboudian, and C. Carraro, Microelectron. Eng. **64**, 479 (2002).
[11] T. Reuter, O. Vidoni, V. Torma, G. Schmid, L. Nan, M. Gleiche, L. Chi, and H. Fuchs, Nano Lett. **2**, 709 (2002).
[12] J. Y. Cheng, F. Zhang, V. P. Chuang, A. M. Mayes, and C. A. Ross, Nano Lett. **6**, 2099 (2006).
[13] D. K. Venkatachalam, D. K. Sood, and S. K. Bhargava, Nanotechnology **19**, 015605 (2008).
[14] Th. Stelzner, G. Andrä, E. Wendler, W. Wesch, R. Scholz, U. Gösele, and C. Christiansen, Nanotechnology **17**, 2895 (2006).
[15] J. M. Poate, D. C. Jacobson, J. S. Williams, R. G. Elliman, and D. O. Boerma, Nucl. Instrum. Methods Phys. Res. B **19**, 480 (1987).
[16] V. Datye and J. S. Langer, Phys. Rev. B **24**, 4155 (1981).
[17] J. S. Langer, Phys. Rev. Lett. **44**, 1023 (1980).
[18] N. H. Fletcher (submitted).